Size distribution of cell pattern observed in gravitational instability

Michiko Shimokawa,[1,*] Hiroyuki Kitahata,[2,3] and Tatsunari Sakurai[2]
[1]*Center for Frontier Science, Chiba University, 1-33, Yayoi-cho, Inage-ku, Chiba-shi, Chiba 263-8522, Japan*
[2]*Department of Physics, Graduate School of Science, Chiba University, 1-33, Yayoi-cho, Inage-ku, Chiba-shi, Chiba 263-8522, Japan*
[3]*PRESTO JST, 4-1-8 Honcho, Kawaguchi, Saitama 332-0012, Japan*
(Received 9 July 2012; published 3 January 2013)

Gravitational instability occurs at the interface of two solutions when a higher-density solution (HDS) is placed on the surface of a lower-density solution (LDS). As the HDS sinks, a cell pattern forms on the surface. We investigate the size distribution of the cells in this pattern. We show that the cumulative size distribution obeys a power law with a power index that is independent of time as long as it is possible to neglect the interactions among the cells. To understand the power law mechanism, a simple model excluding the interactions is proposed, and we demonstrate that this simple model provides the power law measured in experiments. Our results indicate that independent cell generation and growth are key factors to understand the feature of the cell pattern.

DOI: 10.1103/PhysRevE.87.012903 PACS number(s): 89.75.Kd, 89.75.Fb

I. INTRODUCTION

The power law in physics is one of the most familiar rules for critical phenomena [1,2]; the specific heat, magnetic susceptibility, and correlation length all obey a power law and diverge at a critical point in an equilibrium system. The behavior at the critical point can be explained using the free energy obtained in a symmetry assumption [1], and an analysis of the minimum free energy leads to the specific power law around the critical point.

Power law appears not only in an equilibrium system but also in a nonequilibrium system in nature: the frequency distribution of earthquakes [3,4], node number distribution of an internet link [5,6], fragment mass (or size) distribution of glass [7,8], frequency distributions of word and family names [9,10], and diameter distribution of moon craters [2]. The existence of power law means that the system has no characteristic length, which is an anomalous feature. It is thought that the power law is derived from complex behaviors with strong interactions. For a system in a nonequilibrium condition, it is difficult to define the free energy involved in these complex dynamics. Therefore, understanding the power law in a nonequilibrium system has been an interesting topic [2].

Recently, fractal and cell patterns were observed in gravitational instability experiments [11,12]. When a droplet of a higher-density solution (HDS) is placed on the surface of a lower-density solution (LDS), the HDS spreads over the surface of the LDS. Following this, a gravitational instability occurs at the interface between the HDS and LDS, and the HDS sinks, exhibiting a fractal or cell pattern at the interface. In this paper, we focus on the cell pattern that is formed when the HDS sinks. In an investigation of a size distribution of cells, it is found that the number of cells with an area S decreases with increasing S according to a power law. Our aim here is to understand the power law mechanism of the cell size distribution through detailed measurements of the cell pattern development. Clarifying the mechanism will assist in an understanding of not only the cell pattern formation by a gravitational instability but also other phenomena in a nonequilibrium system.

II. EXPERIMENTAL PROCEDURE

For the gravitational instability experiments, glycerin solution and a magnetic fluid are used as the LDS and HDS, respectively. The glycerin solution with 1.21 g/ml consists of glycerin (Wako; 100.50 g), white watercolor (Kokuyo), and water. White watercolor (0.50 g) is dissolved in 100 g of water in order to visualize the surface pattern. In the uniform mixture of these solutions, which are glycerin, white watercolor, and water, the glycerin solution is made. The density of the HDS magnetic fluid (Taiho Kozai, Ferri Colloid W-40) is 1.40 g/ml. Clear snapshots of the surface pattern are obtained as the colors of the HDS and LDS are black and white, respectively.

The LDS is poured into a circular container with a radius of $r = 50$ mm and a height (depth) of $h = 25$ mm, as shown in Fig. 1. The container stands for 10 min or more until the LDS comes to rest. A droplet of the HDS is then placed with a pipette on the surface of the LDS in the center of the container, as shown in Fig. 1. The cell pattern is captured by using a digital video camera (Sony HDR-FX1) with a macro lens (Raynox DCR-150) from above.

III. RESULTS AND DISCUSSION

A. Size distribution of cell pattern

At first, we focus on a time process of a cell pattern. The photographs in Figs. 2(a)–2(e) are snapshots of the cell patterns at $t = 19$, 59, 86, 145, and 206 s after a droplet of the HDS is placed on the surface. These pictures show how the cell pattern develops: (i) The HDS spreads over the surface soon after being placed on the surface [Fig. 2(a)]. (ii) Cells are then generated randomly in space and time on the surface after a large cell emerges at the center, and each cell then grows simultaneously over time [Figs. 2(b)–2(d)]. (iii) The generation and growth rates decrease and become saturated. A stable cell pattern is then observed as shown in Fig. 2(e). This pattern is present for 400 s before finally disappearing.

*shimokawa@physics.s.chiba-u.ac.jp

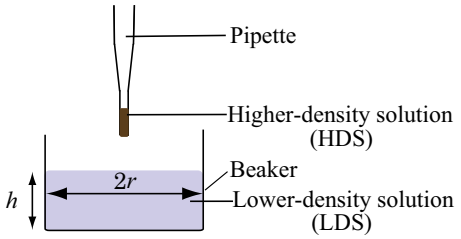

FIG. 1. (Color online) Schematic drawing of the experimental procedure. The radius of the beaker and depth of the glycerin solution (LDS) are shown as r and h, respectively.

These cells have several sizes as shown in upper photographs of Fig. 2. The size distribution of the cells in each photograph is shown in the corresponding plot in Fig. 2. Lower pictures of Fig. 2 show the results of the cumulative distribution of the number of cells with the area more than S,

$$F(S;t) = \int_S^{+\infty} f(S';t)\,dS', \tag{1}$$

where $f(S';t)$ is the number of cells with area S' at an elapsed time t. The maximum value of $F(S;t)$ corresponds to total number of cells $N(t)$ at t. And, $N(t)$ is 4, 46, 65, 94, and 97 at $t = 19$, 59, 86, 145, and 206 s, respectively. Furthermore, the cumulative size distributions show that S varies from 0.03 to 308 mm^2. The distribution $F(S;t)$ for Figs. 2(b) and 2(c) decay according to the power law $\ln[F(S;t)] \sim -A \ln S$, where A is a constant. The power index A was determined subject to the following conditions: (i) The fit is performed for $S \gtrsim 0.5$ mm^2, since data for $S \lesssim 0.5$ mm^2 are so small that $f(S;t)$ contains a large error. (ii) The fitting range has over one digit. (iii) The fitting provides the minimum variance in the measurements through a least-squares method in which the fitting was varied for several trials. The solid lines in Figs. 2(b) and 2(c) show the results of the fit for A, where the values of A are 0.80 and 0.83, respectively. The line for $A = 0.80$ is shown as the dashed lines

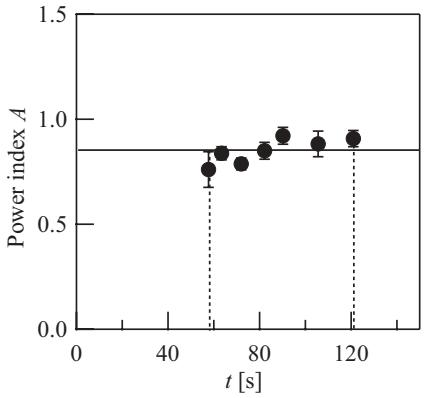

FIG. 3. Time series of the power index A in the experiments for $r = 50$ mm and $h = 25$ mm. The closed circles and the solid line show the experimental data and average value ($A = 0.85$), respectively. A power law is observed during the time range between two dashed lines.

also in Figs. 2(d) and 2(e). A comparison of the experimental data and the fit indicates that the behavior of the experimental data in Figs. 2(d) and 2(e) is different from that in Figs. 2(b) and 2(c). Thus, only distributions at a small elapsed time are described well by a power law. To clarify the exact time range, $F(S;t)$ was investigated for various t. A fitting by a power law is suitable for 59 s $\lesssim t \lesssim$ 120 s, which is between dashed lines in Fig. 3. The discussion on the fitting range is shown in Sec. III D. Figure 3 shows a time series of the power index A, and the average value $A = 0.85 \pm 4.7 \times 10^{-2}$ is shown as the solid line. Over the fitted time range, there is little variation in the value of A from the average value.

B. Number of cells and the area

Here, we focus on the formation process of the cell pattern at $t \lesssim 120$ s when the similar power index $A = 0.85$ is measured.

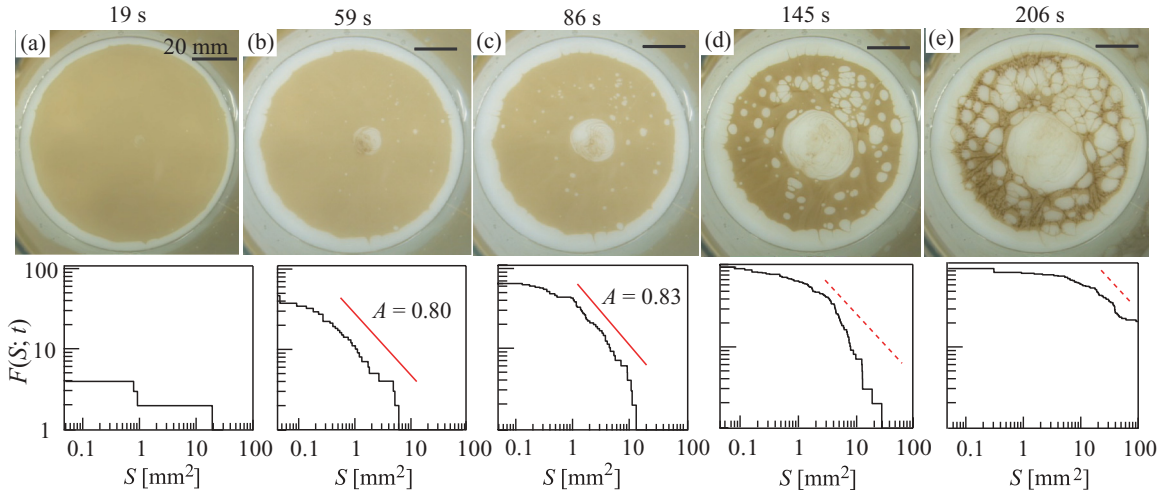

FIG. 2. (Color online) Cell pattern development and cumulative size distribution of the cells in experiments with $r = 50$ mm and $h = 25$ mm. The photographs show the surface pattern captured at elapsed time (a) 19 s, (b) 59 s, (c) 86 s, (d) 145 s, and (e) 206 s after a droplet of the higher-density solution is placed on the surface. The plots show the corresponding the cumulative size distribution $F(S;t)$ of the cells. The solid lines in the plots for (b) and (c) are fits to a power law $\ln[F(S;t)] \sim -A \ln(S)$, where A is a constant. The dashed lines in (d) and (e) are the plots for $A = 0.80$.

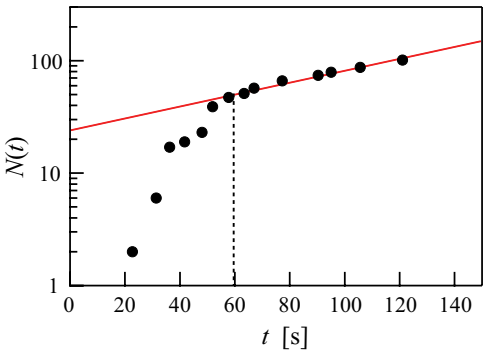

FIG. 4. (Color online) Number of cells $N(t)$ at elapsed time t after a droplet of higher-density solution is placed on the surface measured in the experiment for $r = 50$ mm and $h = 25$ mm. The solid line shows the fit to an exponential function. The dashed line shows a time when the data start to be fitted with an exponential function.

As the generation and the growth of cells are characteristics of the cell pattern formation, shown in upper pictures of Fig. 2, we also examine the number of cells and the area of each cell in this time range.

Figure 4 shows a time series of the number of cells $N(t)$. The number $N(t)$ increases according to an exponential function $\exp(at)$ for 60 s $\lesssim t \lesssim$ 120 s, where $a = (1.30 \pm 0.04) \times 10^{-2}$ s^{-1}. Accurate analysis is difficult, since the cell area is too small at $t \lesssim 60$ s. Therefore, we focus on the data for $t \gtrsim 60$ s. The behavior at small t was investigated in experiments with a high-resolution camera, and a similar result was also obtained [13].

Figure 5 shows the area of the ith cell. Four cells ($i = 1$, 2, 3, 4), shown in Fig. 5(a), were analyzed. These cells were spatially separated from other cells and appeared to grow independently. The analyses provided the area $S_i(t)$ of the ith cell at t in Fig. 5(b). As shown in Fig. 5(b), the generation time τ_i for individual cells varies between 22 and 80 s. As mentioned in Sec. III A, we regarded that the data at $S_i(t) \gtrsim 0.5$ mm^2 were possible to be analyzed. Now, we define that the cell generates at the time when its area reaches $S_0 = 0.5$ mm^2. Then, the elapsed time after the ith cell generates is denoted as t_i', where $t_i' = t - \tau_i$ and $t_i' = 0$ s at $S_0 = 0.5$ mm^2. Figure 5(c) shows a development of $S_i(t_i')/S_0$ with t_i'. The data for the ith cell correspond to those in Fig. 5(b). Although each cell generates at a different time and grows in a different region, $S_i(t_i')/S_0$ is quite similar [Fig. 5(c)]. This result demonstrates that the cells grow independently. The data for $S_i(t_i')/S_0$ are consistent with the exponential function $\exp(bt_i')$ for $t_i' \lesssim 120$ s, shown as the solid line in Fig. 5(c). The average value of b for cells $i = 1$–4 is $b = (1.8 \pm 0.3) \times 10^{-2}$ s^{-1}. Hereafter, we denote $S_i(t_i')$ as $S(t') = S_0 \exp(bt')$, since the tendency does not depend on individual cells. The data in experiments with a high-resolution camera provide $S(t') = S_0 \exp(bt')$ in the condition that even the area is smaller than 0.5 mm^2. And, the b is 1.73×10^{-2} s^{-1}, which is a close value to $b = 1.80 \times 10^{-2}$ s^{-1} in Fig. 5(c) [13].

C. Simple model to lead a power law

Now, our aim is to understand the mechanism of the power law $F(S;t) \sim S^{-A}$ for $t \lesssim 120$ s, where a similar power index is measured. The experimental results in Figs. 4 and 5 suggest the following:

(i) The number of cells increases with time according to

$$N(t) \sim \exp(at) \tag{2}$$

at 60 s $\lesssim t \lesssim$ 120 s, and (ii) the area of each cell grows according to

$$S(t') = S_0 \exp(bt'). \tag{3}$$

Equation (3) shows that $S(t')$ is determined uniquely for t'. This allows $dt' = \frac{\partial t'}{\partial S} dS$, and leads to

$$N(t) = \int_0^t n(\tau) d\tau = \int_0^t n(t - t') dt' = \int_{S_0}^{S_0 \exp(bt)} n(t - t') \frac{\partial t'}{\partial S} dS, \tag{4}$$

where the generation time of cells and the generated number of cells at τ are $\tau = t - t'$ and $n(\tau) = dN(\tau)/d\tau$, respectively. On the other hand, $f(S;t)$ is the number of cells with area S

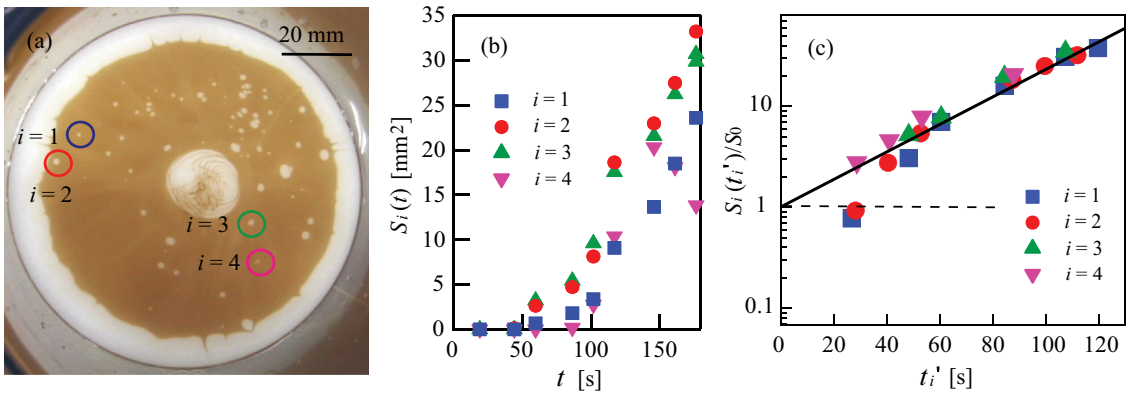

FIG. 5. (Color online) Time series of the area of individual cells in experiments for $r = 50$ mm and $h = 25$ mm. (a) Snapshot of investigated four cells ($i = 1$, 2, 3, 4) at an elapsed time $t = 86$ s after a droplet of the higher-density solution is placed on the surface of the lower-density solution. The data for individual cells are indicated by different symbols in (b) and (c). (b) Time development of area $S_i(t)$ of ith cell at t. (c) Time development of $S_i(t_i')/S_0$ for individual cells, where $S_0 = 0.5$ mm^2 and $t_i' = 0$ s as $S_i = S_0$. The solid line represents a fit to an exponential function. The dashed line shows $S_i = S_0$.

at t according to Eq. (1). Then,

$$N(t) = \int_0^{+\infty} f(S;t)dS = \int_{S_0}^{S_0 \exp(bt)} f(S;t)dS, \quad (5)$$

because from Eq. (3) the minimum and maximum values of S at t are S_0 and $S_0 \exp(bt)$, respectively. A comparison of Eq. (4) and Eq. (5) yields

$$n(t-t')\frac{\partial t'}{\partial S} = f(S;t) \quad (6)$$

for an arbitrary time. Equations (2) and (3) lead Eqs. (7) and (8), respectively:

$$n(t-t') = \frac{dN(t-t')}{d(t-t')} \sim a \exp[a(t-t')], \quad (7)$$

$$t' = \ln\left(\frac{S(t')}{S_0}\right)^{1/b}, \quad (8)$$

because $\ln S(t') = \ln S_0 + bt'$ according to Eq. (3). The Eq. (8) yields

$$\frac{\partial t'}{\partial S} = \frac{1}{bS}. \quad (9)$$

Using Eqs. (7)–(9), Eq. (6) gives

$$\begin{aligned} f(S;t) &\sim a \exp\{a(t-t')\}\frac{1}{bS} \\ &= a \exp(at) \exp\left\{-a \ln\left(\frac{S}{S_0}\right)^{1/b}\right\}\frac{1}{bS} \\ &= \frac{a}{bS_0} \exp(at)\left(\frac{S}{S_0}\right)^{-a/b-1} \sim \exp(at) S^{-a/b-1}. \end{aligned} \quad (10)$$

Now, the cumulative size distribution at each time is considered. The factor $\exp(at)$ is nonessential for the distribution at $60\ \mathrm{s} \lesssim t \lesssim 120\ \mathrm{s}$ when the power law is measured. Therefore, $f(S;t)$ is regarded as $S^{-a/b-1}$. The cumulative distribution $F(S;t)$ is

$$F(S;t) = \int_S^{+\infty} f(S';t)dS' \sim S^{-a/b}. \quad (11)$$

Equation (11) shows that the cumulative distribution $F(S;t)$ obeys a power law. This result agrees with the experimental results shown in Fig. 2. Furthermore, the power index a/b is independent of time, which also agrees with the results of A shown in Fig. 3.

The power index a/b is compared with A for several depths of the circular container h. Since a cell pattern appears only at $h \lesssim r = 50$ mm [12], $F(S;t)$ was investigated for $h \leqslant 40$ mm. The results are shown in Fig. 6(a), where the closed circles and open triangles represent A and a/b, respectively. The value of a/b is 0.72 ± 0.27 at $h = 25$ mm ($a = (1.30 \pm 0.04) \times 10^{-2}\ \mathrm{s}^{-1}$ and $b = (1.8 \pm 0.3) \times 10^{-2}\ \mathrm{s}^{-1}$), which is close to the value $A = 0.85 \pm 4.7 \times 10^{-2}$ at $h = 25$ mm found in Fig. 3. The value of a/b also shows agreement with A for other h. These results indicate that Eqs. (2) and (3) as the fitting are reasonable and lead to the conclusion that independent generation and growth are important for the cell pattern formation.

We also note that the power index A increases with increasing h. Figure 6(b) shows the change in both a and b as a function of h, where a^{-1} and b^{-1} are indexes of Eqs. (2) and (3). The index a is almost constant, while b tends to decrease with increasing h. This result anticipates that a is a parameter derived from the gravitational instability. Since the disturbance due to a gravitational instability depends only on the surface condition such as densities and interfacial tension between the HDS and LDS [14], a must be independent of h. In contrast, it is thought that b explains the hydrodynamic effect in the global experimental system because the flow of the HDS and LDS brings about the cell growth. However, measurements of the flow field will be needed in order to confirm this hypothesis. The measurement remains as a future subject.

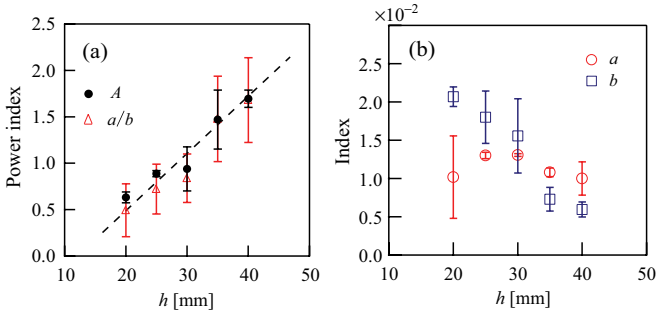

FIG. 6. (Color online) (a) Power index for the depth h. The closed circles and open triangles show the experimental results for A and a/b obtained from our model, respectively. The dashed line is an approximate straight-line fit. (b) The indexes a (open circles) and b (open squares) for different h.

D. Occupancy of cells

As we have demonstrated, the assignment $A \sim a/b$ is valid only for $t \lesssim 120$ s in experiments with $h = 25$ mm. To clarify the behavior at $t \gtrsim 120$ s, the occupancy $p(t)$ of the cells was investigated. Figure 7 shows $p(t) = \sum_i S_i(t-\tau_i)/B$ at t, where $S_i(t-\tau_i)$ and B represent the area of the ith cell at t and the whole region surrounded by the edge of the cell pattern, respectively. The area $S_i(t-\tau_i)$ can be defined at $t \geqslant \tau_i$, and thus it is regarded as zero otherwise. The B is almost constant

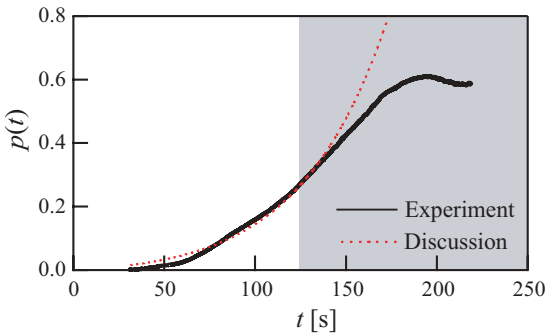

FIG. 7. (Color online) Occupancy p of all cells for a whole area B of a cell pattern at t, where $p(t) = \sum_i S_i(t-\tau_i)/B$. The data are measured in experiments for $r = 50$ mm and $h = 25$ mm. The solid and dashed lines are the data obtained from our experiments and Eq. (12), respectively. After 130 s, the agreement between the experimental data and those of Eq. (12) diminished. This region is shown in grey.

as shown in Fig. 2. The experimental result is shown as a solid line in Fig. 7. As shown in Fig. 7, $p(t)$ increases with increasing t and is saturated at $t \sim 190$ s.

Equations (2) and (3) also lead $p(t)$. The occupancy can be expressed as

$$\begin{aligned} p(t) &= \frac{\int_0^t n(\tau)S(t-\tau)d\tau}{B} = \frac{1}{B}\int_0^t \frac{dN(\tau)}{d\tau}S(t-\tau)d\tau \\ &\sim \frac{S_0}{B}\int_0^t a\exp(a\tau)\exp\{b(t-\tau)\}d\tau \\ &= \frac{S_0 a}{B(a-b)}\exp(bt)[\exp\{(a-b)t\}-1] \\ &= \frac{S_0 a}{B(a-b)}\{\exp(at)-\exp(bt)\} \\ &= C\{\exp(at)-\exp(bt)\}, \end{aligned} \tag{12}$$

where values of a and b were obtained from those of Figs. 4 and 5(c). The fitting function, provided by Eq. (12), is $C\{\exp(at)-\exp(bt)\}$, where $C = -6.08 \times 10^{-2}$. The value of C is determined in the measurement through a least-squares method, and the fitting region is at 60 s $\lesssim t \lesssim$ 140 s. As a is smaller than b in the condition of $h = 25$ mm, $C < 0$ is reasonable. The plot of the fitting function is shown as the dashed line in Fig. 7, and the region in which the dashed line deviates from the solid line of the experimental data is represented by the grey shading. The transition occurs around at $t = 130$ s, which is close to 120 s. This result suggests that a different mechanism from that discussed for $t \lesssim 120$ s is needed for $t \gtrsim 120$ s. The cell generation and growth rate might decrease, since the experimental value is lower than that of Eq. (12) for $t \gtrsim 120$ s. For $t \gtrsim 120$ s, the interaction among the cells is considered to be one of the reasons for the difference between the two results. As seen in Figs. 2(d) and 2(e), a cell structure with a large $p(t)$ prevents the growth of cells. This effect must first appear at $t \sim 120$ s, and so therefore, the common power index is obtained only for $t \lesssim 120$ s. The pattern formation with a strong interaction for $t \gtrsim 120$ s is a topic of future research.

IV. SUMMARY

When a droplet of HDS is placed on a LDS surface, the HDS spreads over the LDS surface. A gravitational instability occurs at the HDS–LDS interface, and the HDS sinks. During the sinking process, a cell pattern is formed on the surface. We have investigated the cumulative size distribution of the cells and found that the distribution obeys a power law as shown in Fig. 2. The power index is independent of time as shown in Fig. 3, as long as an interaction among the cells is neglected. Experimental measurements in the time region without the interaction yielded the following conclusions: (i) the number of cells increases with time according to an exponential function (Fig. 4), and (ii) the area of each cell grows independently according to an exponential function [Fig. 5(c)]. These results lead to a power law with a power index that agrees with that obtained from our experiments. We also found good agreement between power indexes of experiments and those of our discussion for different LDS depths as shown in Fig. 6(a). These results indicate that independent cell generation and growth are key factors to understand the feature of a cell pattern.

ACKNOWLEDGMENTS

We thank Professor Honjo, Professor Ohta, and Professor Sakaguchi, members of Honjo Laboratory, as well as Professor Takami, Professor Yamamoto, Professor Ito, Professor Teramoto, Dr. Sakaki, Professor Kumagai, Dr. Homma, K. Takimoto, and K. Shimokawa for fruitful discussions and helpful suggestions. This work was supported by JSPS KAKENHI Grant No. 23540454, Sumitomo Foundation Grant, and the JSPS Core-to-Core program "International research network for non-equilibrium dynamics of soft matter."

[1] H. E. Stanley, *Introduction to Phase Transitions and Critical Phenomena* (Oxford University Press, Oxford, 1971).
[2] N. E. J. Newman, Contemp. Phys. **46**, 323 (2005).
[3] B. Getenberg and C. F. Richter, Ann. Geophys. **9**, 1 (1956).
[4] Y. Y. Kagan, Pure Appl. Geophys. **155**, 537 (1999).
[5] A.-L. Barabási and R. Albert, Science **286**, 509 (1999).
[6] A.-L. Barabási, R. Albert, and H. Jeong, Physica A **272**, 173 (1999).
[7] Y. Hayakawa, Phys. Rev. B **53**, 14828 (1996).
[8] H. Katsuragi, D. Sugino, and H. Honjo, Phys. Rev. E **68**, 046105 (2003).
[9] G. K. Zipf, *Human Behaviour and the Principle of Least Effort* (Addison-Wesley, Reading, MA, 1949).
[10] S. Miyazima, Y. Lee, T. Nagamine, and H. Miyajima, Physica A **278**, 282 (2000).
[11] M. Shimokawa and S. Ohta, Fractals **20**, 97 (2012).
[12] M. Shimokawa, J. Phys. Soc. Jpn. **81**, 094003 (2012).
[13] See Supplemental Material at http://link.aps.org/supplemental/10.1103/PhysRevE.87.012903 for results obtained using a high-resolution camera.
[14] S. Chandrasekhar, *Hydrodynamic and Hydromagnetic Stability* (Oxford University Press, Oxford, 1961).